



## Experimental study on bubble and droplet entrainment in vertical churn and annular flows and their relationship

Zhennan Zhang <sup>a,b</sup>, Zhiyuan Wang <sup>a</sup>, Hui Liu <sup>a</sup>, Yonghai Gao <sup>a</sup>, Hao Li <sup>a</sup>, Baojiang Sun <sup>a,\*</sup>

<sup>a</sup>School of Petroleum Engineering, China University of Petroleum (East China), 66 Changjiang West Road, Qingdao 266580, China

<sup>b</sup>Shandong Provincial Key Laboratory of Oil & Gas Storage and Transportation Security, China University of Petroleum (East China), Qingdao 266555, China



### HIGHLIGHTS

- Bubble and droplet entrainment are experimentally identified for vertical churn and annular flows.
- The intensity distribution of entrainment is described.
- The relationship between related entrainments is discussed.
- The bubble and droplet entrainment regime is given.

### ARTICLE INFO

#### Article history:

Received 4 January 2019

Received in revised form 17 April 2019

Accepted 5 May 2019

Available online 6 May 2019

#### Keywords:

Bubble entrainment

Droplet entrainment

Churn flow

Annular flow

High-speed camera

### ABSTRACT

Bubble and droplet entrainment plays an important role in the mass transfer between the liquid film and the gas core in churn and annular flow. In this work, bubble and droplet entrainments in vertical churn and annular flows are systematically studied in an air-water two-phase vertical flow experiment using a high-speed camera. The results show that there are three kinds of bubble entrainment and five kinds of droplet entrainment in churn and annular flows. The entrainment can be categorized as primary entrainment and secondary entrainment. The primary entrainment includes one kind of bubble entrainment, which is a large wave roll and overturn, and three kinds of droplet entrainment, which are shearing-off of waves containing bubbles, bag break-up of waves, and ligament break-up of waves. The secondary entrainment includes two kinds of bubble entrainment, which are synchronized bubble entrainment along with droplet entrainment and droplets from the gas core impacting the liquid film, and two kinds of droplet entrainment, which are droplets impacting the liquid film and the burst of bubbles. With the flow pattern transition from churn to annular flow, the dominant bubble entrainment changes from large wave roll and overturn to the synchronized bubble entrainment along with droplet entrainment accompanied by a decreasing intensity. The dominant droplet entrainment changes from shearing-off of waves containing bubbles to ligament break-up of waves with the intensity first decreasing and then increasing. There is a close relationship between bubble entrainment and droplet entrainment. The entrained bubbles reduce the strength of large-scale waves and facilitate the shearing-off of waves. A small number of droplets are entrained due to the burst of residual bubbles in the liquid film. Droplets that are generated by bag or ligament break-up of waves can directly impact the nearby liquid film, leading to synchronous bubble entrainment. A small number of bubbles can be entrapped by droplets from the gas core impacting the liquid film. The primary entrainment intensity is significantly greater than that of the secondary entrainment. With the transition from churn to annular flow, the change in the primary entrainment intensity determines the variety of the secondary entrainment intensity.

© 2019 Elsevier Ltd. All rights reserved.

### 1. Introduction

Vertical gas-liquid pipe flow exists widely in chemical and petroleum engineering. The flow pattern is usually classified into bub-

ble flow, slug flow, churn flow, and annular flow (Taitel et al., 1980; Wu et al., 2017). In churn and annular flows, continuous fluid exists for both liquid and gas phases, which are the liquid film flowing along the tube wall and the central gas core, respectively (Dasgupta et al., 2017; Hewitt, 2012). The interaction between the liquid film and the gas core leads to continuous mass transfer between these two continuous fluids (Alipchenkov et al., 2004;

\* Corresponding author.

E-mail address: [sunbj1128@126.com](mailto:sunbj1128@126.com) (B. Sun).

## Nomenclature

|            |   |              |  |
|------------|---|--------------|--|
| $D$        | pipe diameter, m  | $U_{sl}$     | superficial liquid velocity, m/s   |
| $Fr_g$     | gas Froude number, dimensionless  | $We_\delta$  | liquid film Weber number, dimensionless                                    |
| $Fr_l$     | liquid Froude number, dimensionless   |              |  |
| $G$        | gravitational acceleration, $9.8 \text{ m/s}^2$                                 |              |  |
| $Ku$       | Kutateladze number, dimensionless   |              |  |
| $N_\mu$    | viscosity number, dimensionless   |              |  |
| $Re_{lf}$  | liquid film Reynolds number, dimensionless                                      | $\delta$     | liquid film thickness, m   |
| $Re_{sg}$  | superficial gas Reynolds number, dimensionless                                  | $\Delta\rho$ | density difference between the liquid phase and gas phase, $\text{kg/m}^3$ |
| $Re_{sl}$  | superficial liquid Reynolds number, dimensionless                               | $\rho_g$     | gas density, $\text{kg/m}^3$   |
| $U_{sg}$   | superficial gas velocity, m/s   | $\rho_l$     | liquid density, $\text{kg/m}^3$  |
| $U_{sg-c}$ | critical superficial gas velocity corresponding to the droplet entrainment, m/s | $\mu_l$      | liquid dynamic viscosity, $\text{Pa}\cdot\text{s}$                         |
|            |   | $u_{lf}$     | liquid film velocity, m/s  |
|            |   | $\sigma$     | surface tension, N/m   |

Kataoka et al., 2000; Patruno et al., 2009). For adiabatic flow, the mass exchange includes droplet entrainment where the liquid film is entrapped by the gas core and dispersed as droplets in the gas core and bubble entrainment where the gas core is trapped by the liquid film and is dispersed as bubbles in the liquid film. The entrainment phenomenon is usually encountered in the situation where there is a gas-liquid interface (Isaenkov et al., 2019; Miwa et al., 2018; Tekavčič et al., 2018; Zhang et al., 2012).

In churn flow, the huge wave makes the droplet entrainment different from that in annular flow (Azzopardi and Wren, 2004). In contrast, Wang et al. (2013a, 2017) proposed that droplet entrainment in churn flow is the same as that in annular flow. Therefore, the droplet entrainment model is basically the same (Liu and Bai, 2017; Wang et al., 2013b).

There are various definitions for droplet entrainment, as listed in Table 1. The droplet entrainment is usually suggested to be the result of a Kelvin-Helmholtz instability (Woodmansee and Hanratty, 1969). The criteria of Ishii and Grolmes (1975) were directly adopted by Ishii and Mishima (1989) and Cioncolini and Thome (2010) to predict the droplet entrainment fraction. The criteria were further simplified by Crowe (2005) into the form of the Kutateladze number. Azzopardi (1983) proposed that the criterion between the bubble break-up and the ligament break-up depends on the liquid film Weber number, which only reflects the general trend (Azzopardi, 1997). Van 't Westende (2008) attributed the two distributions of droplet sizes to these two mechanisms. Pham et al. (2014) proposed that there is a shadow region where both mechanisms coexist. Berna et al. (2014) pointed out that the droplet entrainment condition is always close to the occurrence condition of the disturbance wave within high gas velocities. Kumar et al. (2016) figured out three entrainment routes using a numerical simulation. In addition, the droplet entrainment criterion used by Pan and Hanratty (2002) and Sawant et al. (2008) in correlations of the entrainment fraction is

$$\frac{D^{0.5} U_{sg-c} \left( \rho_1 \rho_g \right)^{0.25}}{\sigma^{0.5}} \simeq 40 \quad (1)$$

where  $D$  is the pipe diameter, m; and  $U_{sg-c}$  is the critical superficial gas velocity corresponding to the droplet entrainment, m/s.

Studies of bubble entrainment in vertical churn and annular flows are relatively scarce even though entrained bubbles can be easily observed (Schubring et al., 2010). At present, bubble entrainment is preliminarily defined only for horizontal flow (Hann et al., 2018; Rodríguez and Shedd, 2004). For vertical flow, van Nimwegen et al. (2015) found that surfactants are highly beneficial to bubble entrainment.

The droplet entrainment criteria are shown on the (Mishima and Ishii, 1984) flow pattern map in Fig. 1. The liquid film thickness is calculated by the (Berna et al., 2014) correlation.

$$\frac{\delta}{D} = 7.165 Re_{sg}^{-1.07} Re_{sl}^{0.48} \left( \frac{Fr_g}{Fr_l} \right)^{0.24} \quad (2)$$

$$Fr_g = \frac{U_{sg}}{\sqrt{gD}} \quad (3)$$

$$Fr_1 = \frac{U_{sl}}{\sqrt{gD}} \quad (4)$$

where  $Re_{sg}$  is the superficial gas Reynolds number, dimensionless;  $Re_{sl}$  is the superficial liquid Reynolds number, dimensionless;  $Frg$  is the gas Froude number, dimensionless; and  $Fr_l$  is the liquid Froude number, dimensionless.

Both Ishii and Grolmes (1975) and Azzopardi (1983) believed that ligament break-up is the dominant droplet entrainment in annular flow. However, the difference between these two criteria becomes larger with increasing  $U_{sg}$ . When the dimensionless (Kumar et al., 2016) criteria are transformed into  $U_{sg}$  and  $U_{sl}$ , the results correspond to more than one curve. Furthermore, these criteria are not distributed in annular flow, which is limited by the setting of its simulation parameters.

High-speed photography is the main experimental research method for studying bubble and droplet entrainment. The purpose of photography is to directly observe the entrainment process and the characteristics of the generated bubbles and droplets (Azzopardi, 1983; Pham et al., 2014, 2015; van Nimwegen et al., 2015; Wang et al., 2017). The flow in the horizontal rectangular duct (Cherdantsev et al., 2014; Patruno et al., 2010) or on rod bundle geometry (Kunugi, 2017; Pham et al., 2014, 2015) is more convenient for intuitive observation. However, there are significant differences. Direct experimental observation of the vertical pipe flow is necessary. Related experiments are restricted within limited flow conditions, which have led to various definitions of entrainment (Cherdantsev, 2018). The numerical method gives a more detailed description of quantitative parameters related to entrainment (Durve and Patwardhan, 2012; Xie et al., 2017). However, the results are limited by the constructed model. There is still a gap between the simulation results and the experimental results.

In this work, the process of bubble and droplet entrainment is defined according to a detailed analysis of the recorded high-speed video. Then, the intensity distribution of each defined entrainment versus the gas and liquid velocities is obtained. The relationship between these is further discussed. The bubble and

**Table 1**

Droplet and bubble entrainment mechanisms for churn and annular flows and the inception criteria.

| Researchers and contents  | Entrainment mechanisms and inception criteria  |
|---|--|
| Hewitt and Hall Taylor (1970)<br>Droplet entrainment<br>Vertical pipe flow  | Breakdown of disturbance waves by undercutting<br>breakdown of disturbance waves by rolling  |
| Ishii and Grolmes (1975)<br>Droplet entrainment<br>Inclined downflow in a rectangular channel with water on a wide wall | Minimum Reynolds number regime, wave undercutting<br>$Re_{lf} < 160$ and $\frac{\mu_l U_{sg}}{\sigma} \sqrt{\frac{\rho_g}{\rho_l}} \geq 1.5 Re_{lf}^{-1/2}$<br>Transition regime, shearing off of roll-wave crests<br>$160 \leq Re_{lf} < 1635$ and $\begin{cases} \frac{\mu_l U_{sg}}{\sigma} \sqrt{\frac{\rho_g}{\rho_l}} \geq 11.78 N_\mu^{0.8} Re_{lf}^{-1/3} & N_\mu \leq \frac{1}{15} \\ \frac{\mu_l U_{sg}}{\sigma} \sqrt{\frac{\rho_g}{\rho_l}} \geq 1.35 Re_{lf}^{-1/3} & N_\mu > \frac{1}{15} \end{cases}$<br>Rough turbulent regime, shearing off of roll-wave crests<br>$Re_{lf} > 1635$ and $\begin{cases} \frac{\mu_l U_{sg}}{\sigma} \sqrt{\frac{\rho_g}{\rho_l}} \geq N_\mu^{0.8} & N_\mu \leq \frac{1}{15} \\ \frac{\mu_l U_{sg}}{\sigma} \sqrt{\frac{\rho_g}{\rho_l}} \geq 0.1146 & N_\mu > \frac{1}{15} \end{cases}$<br>Other mechanisms: liquid impingement, bubble burst, and liquid bulge disintegration<br>$Re_{lf} = \frac{4\rho_l u_{lf}^2}{\mu_l} N_\mu = \frac{\mu_l}{\sqrt{\rho_l \sigma \sqrt{\delta(\rho_l - \rho_g)}}}$ |
| Azzopardi (1983)<br>Droplet entrainment<br>Vertical pipe flow   | Bag break-up of waves, $We_\delta < 25$<br>Ligament break-up of waves, $We_\delta \geq 25$<br>$We_\delta = \frac{\rho_g U_{sg}^2 \delta}{\sigma}$  |
| Crowe (2005)<br>Droplet entrainment<br>Vertical pipe flow   | Minimum Reynolds number regime, $Ku$ increases sharply, entrainment is difficult<br>Transition regime, critical $Ku$ increases to 7.5 with decreasing $Re_{lf}$<br>Rough turbulent regime, $Ku > 3.2$<br>$Ku = \frac{U_{sg}^{0.5}}{(\Delta \rho g \sigma)^{0.25}} U_{sg}$  |
| Kumar et al. (2016)<br>Droplet entrainment<br>Vertical pipe flow  | Orificing, rolling, and undercutting<br>Critical condition (1) (C1), $Re_{lf-K} = -641.45 We_{g-K}^2 + 4117.9 We_{g-K} + 4915.4$<br>Critical condition (2) (C2), $Re_{lf-K} = -62277 We_{g-K}^2 + 85808 We_{g-K} - 8478.8$<br>$We_{g-K} = \frac{\rho_g U_{sg}^2 \delta}{\sigma}$ , $Re_{lf-K} = \frac{\rho_l u_{lf} \delta}{\mu_l}$ , and $We_g$ : 0.003–3, $Re_{lf}$ : 750–12000<br>undercutting resembles bag break-up; rolling resembles ligament break-up<br>Three mechanisms coexist:<br>Bag break-up<br>Ligament break-up<br>Secondary entrainment due to droplet impacts on the film surface  |
| Cherdantsev et al. (2014)<br>Droplet entrainment<br>Gas-sheared liquid film in a horizontal rectangular duct            | Continuous folding action within the disturbance waves<br>Droplet impacting<br>Breakup of bubbles  |
| Rodriguez and Shedd (2004)<br>Bubble entrainment<br>Horizontal pipe flow  | Impacting droplets<br>Impacting of the transitional structures<br>Overturning of the fast ripples  |
| Hann et al. (2018)<br>Bubble entrainment<br>Gas-sheared liquid film in a horizontal rectangular duct                    |  |

droplet entrainment regime maps are constructed individually within the scope of our experiment.

## 2. Experimental apparatus and method

### 2.1. Experimental apparatus

The experimental apparatus is shown in Fig. 2. The experimental apparatus consists of a flow pipe, a gas-liquid supply system, and a measurement and observation device.

The flow pipe is a transparent vertical plexiglass circular tube with an internal diameter of 0.05 m, a wall thickness of 3 mm, and a length of 3.7 m.

Air is injected from the air compressor and through the gas stabilization chamber into the bottom of the vertical tube. The gas flow rate is adjusted as the valve opens. Tap water is injected through the porous pipe wall 0.4–0.5 m downstream of the gas inlet from the gear pump. Circular holes are uniformly distributed on the pipe wall to ensure the stable injection of tap water. The diameter of the hole is 2 mm. The liquid flow rate is adjusted by changing the gear pump speed. The speed of the gear pump is 0–1400 r/min, and the corresponding displacement is 0–3.3 m<sup>3</sup>/h.

The volume flow rate of air and tap water is measured by the rotameter. Two identical gas rotameters are connected in parallel to meet the measurement requirements of the large airflow rate.

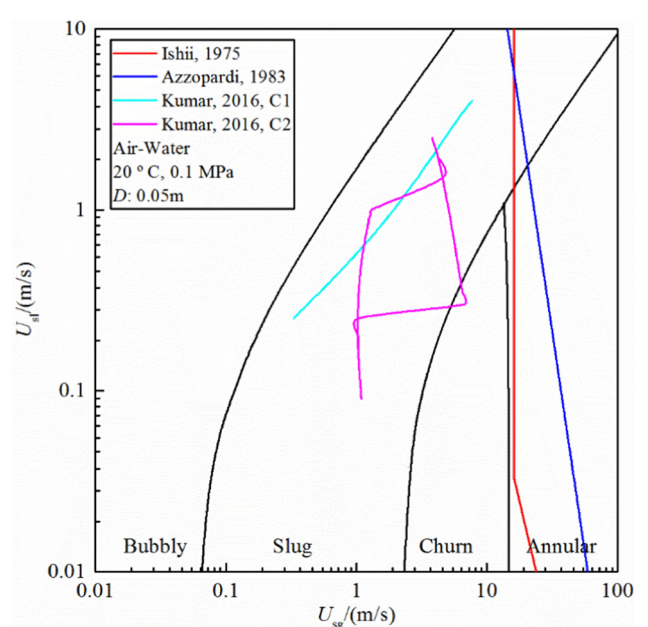
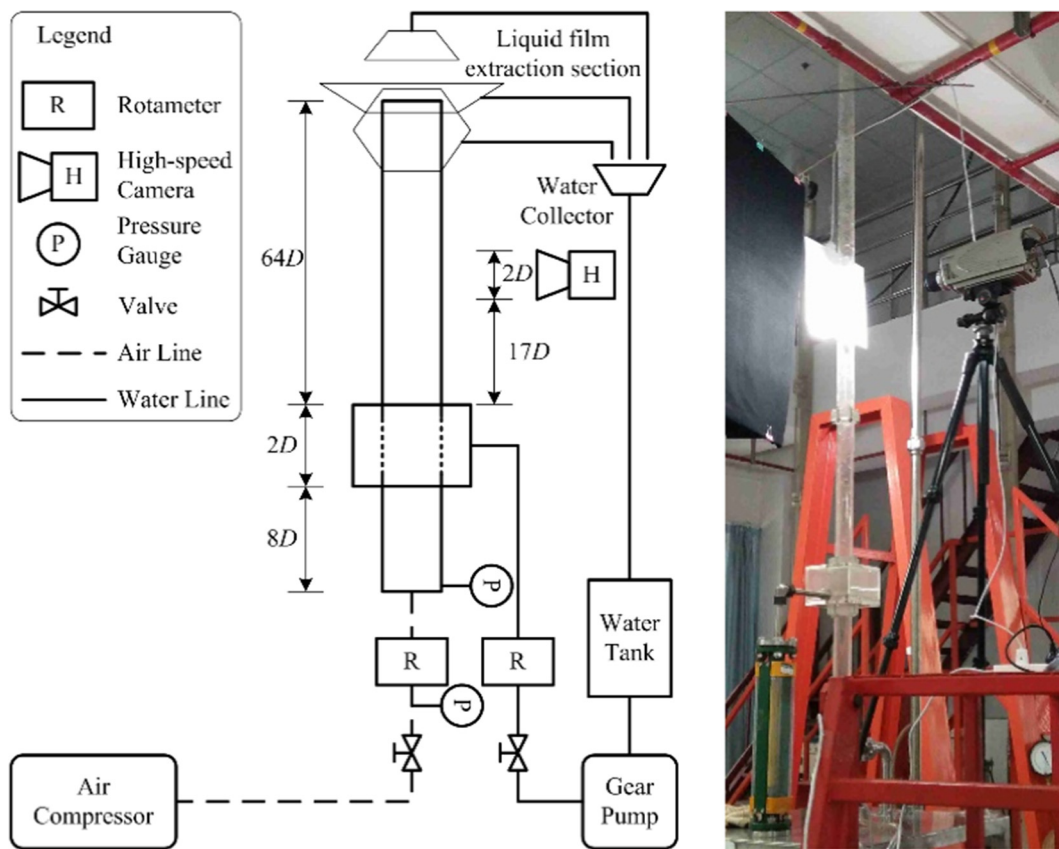


Fig. 1. Droplet entrainment criteria on the Mishima and Ishii (1984) flow pattern map.



**Fig. 2.** The experimental apparatus.

The range of the gas rotameter is 50–250 Nm<sup>3</sup>/h with an accuracy of 1.5% FS. The range of the liquid rotameter is 0.1–1 m<sup>3</sup>/h with an accuracy of 2.5% FS. The range of the pressure gauge upstream of the gas rotameter is 0.6 MPa with an accuracy of 0.4% FS. The range of the pressure gauge at the inlet of the pipe is 10 kPa with an accuracy of 0.4% FS. Air is released into the atmosphere at the pipe outlet, and tap water is collected by a specially designed liquid film extraction section.

An Olympus i-SPEED TR MONO high-speed CMOS camera is used to record the backlight images of the two-phase flow in the pipe, which is placed 0.85 m downstream from the liquid inlet. A white light-emitting diode (LED) is used for backlighting the pipe. In addition, an acrylic light-diffusive sheet is placed between the LED and the pipe to ensure that light shines evenly on the pipe.

## 2.2. Experimental method

The experiment was carried out at room temperature and pressure using air and tap water. There was no phase change under the operating conditions. The mass exchange between the liquid film and the gas core were only the mechanical mass transfer. This work focused on bubble and droplet entrainment.

Experiments at 55 different flow conditions with 11 superficial gas velocities and 5 superficial liquid velocities were carried out. The superficial velocity is calculated based on the measured flow rate. The measured gas flow rate must be corrected according to the pressure upstream of the gas rotameter. The superficial gas velocity ranged from 10.8 to 60.3 m/s, and the superficial liquid velocity ranged from 0.02 to 0.071 m/s.

A high-speed camera was used to capture the entrainment characteristics of the bubble and droplet from the side of the tube with a range of 0.85–0.95 m downstream from the top of the liquid

inlet. Because entrainment is only related to the gas-liquid interaction, there is no need to ensure that the flow in the observation location is fully developed. At a fixed liquid flow rate, the gas flow rate is adjusted to the set value in the order of smallest to largest in magnitude. When the flow is stable under each flow condition, the videos are made at 2000 fps with a resolution of 1280 × 1024. The pixel size is 0.021 mm.

Due to the complexity of the entrainment process, there is no automatic processing method to deal with the high-speed video at this stage. To determine the process and behavior of each entrainment, only the artificial method is feasible. It is sufficient to acquire knowledge about the distribution characteristics of every entrainment process with flow conditions. Therefore, the entrainment process and its occurrence intensity are defined artificially in this paper. The entrainment process is determined and defined according to a unique phenomenon induced during the related entrainment, which is further described in the corresponding section. The entrainment intensity is preliminarily determined according to the frequency of occurrence, occurrence area, and the number and size of the entrained bubbles or droplets. The entrainment intensity is divided into five grades ranging from zero to four. Zero indicates that there is no entrainment, and four represents the highest intensity of entrainment observed in our experiment.

## 3. Results and discussion

The bubble and droplet entrainments are the result of the gas-liquid phase hydrodynamic interaction. They vary with the flow pattern transition. In this paper, we focus on the way of bubble and droplet entrainments and their intensity distribution change with changes in gas and liquid velocities. Therefore, the flow

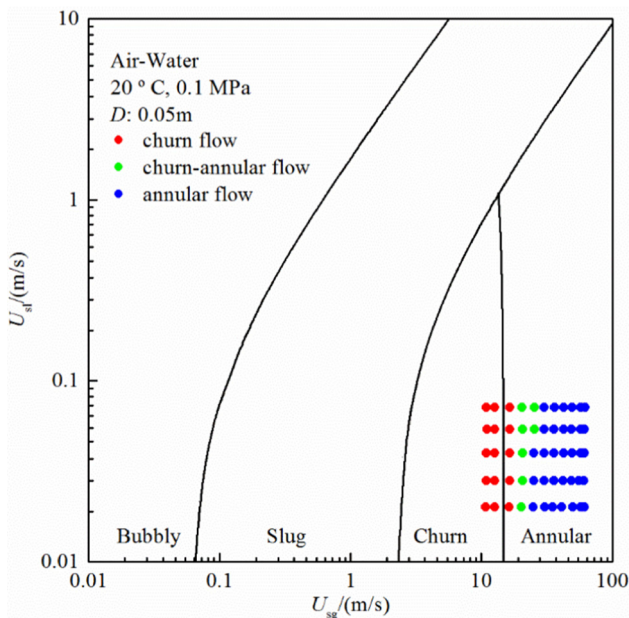


**Fig. 3.** Distribution of experimental range on the Mishima and Ishii (1984) flow pattern map.

regime is identified first. The way of entrainment is defined and recognized, and the intensity is then statistically analyzed.

The distribution of the observed flow regimes in the (Mishima and Ishii, 1984) flow pattern is shown in Fig. 3. There are three flow regimes under the experimental conditions: churn flow, churn-annular flow, and annular flow. The transition boundary is similar to that in the flow pattern.

The distributions of the wave and base liquid film versus with flow conditions are shown in Fig. 4. There are three wave regimes for the interfacial waves: the ripple regime, the disturbance and ripple regime, and the intermittent flow surface regime (Salque et al., 2013). Meanwhile, there are three kinds of interfacial waves: ripple, disturbance wave, and huge wave (Hewitt, 2012). The dis-

turbance is a circumferentially uniformly distributed cluster formed by the aggregation of multiple wave elements, which is the ripple (Alekseenko et al., 2014). Different types of waves play different roles in bubble and droplet entrainment.

As a whole, the axial distribution range of the interfacial wave decreases with the increase in superficial gas velocity. The distribution range refers to the area of the region that the wave covers. At high superficial gas velocities, the interfacial wave presents a uniform circumferential strip shape. In contrast, the axial distribution range of the interfacial wave increases with the increase in the superficial liquid velocity. With the increase in the superficial gas velocity, the thickness of the base liquid film increases. However, the wave height decreases with an increasingly even distribution. With the increase in the superficial liquid velocity, the wave height increases, and huge waves with incomplete circumferences appear.

With the increase in the superficial gas velocity, the number density of entrained bubbles in the liquid film decreases together with the decrease in bubble size. When the superficial gas velocity decreases to a certain extent, there are no entrained bubbles in the liquid film. With the increase in the superficial liquid velocity, both the number density and the size of the entrained bubbles in the liquid film increase. This indicates that the increase in the superficial liquid velocity is beneficial to the bubble entrainment; however, the increasing superficial gas velocity constrains the intensity of the bubble entrainment.

With the increase in the superficial gas velocity, the size of the wave element decreases, and the aspect ratio gets smaller. This indicates that the intensity of droplet entrainment increases. In contrast, the change reverses with the increase in the superficial liquid velocity.

Both bubble and droplet entrainment change substantially when the flow regime transits from churn to annular flow. Furthermore, the interaction characteristics between bubble entrainment and droplet entrainment also change. These will be discussed in detail in the following section.

### 3.1. Bubble entrainment

There are three kinds of bubble entrainment observed in churn and annular flows within the experimental range: the large wave

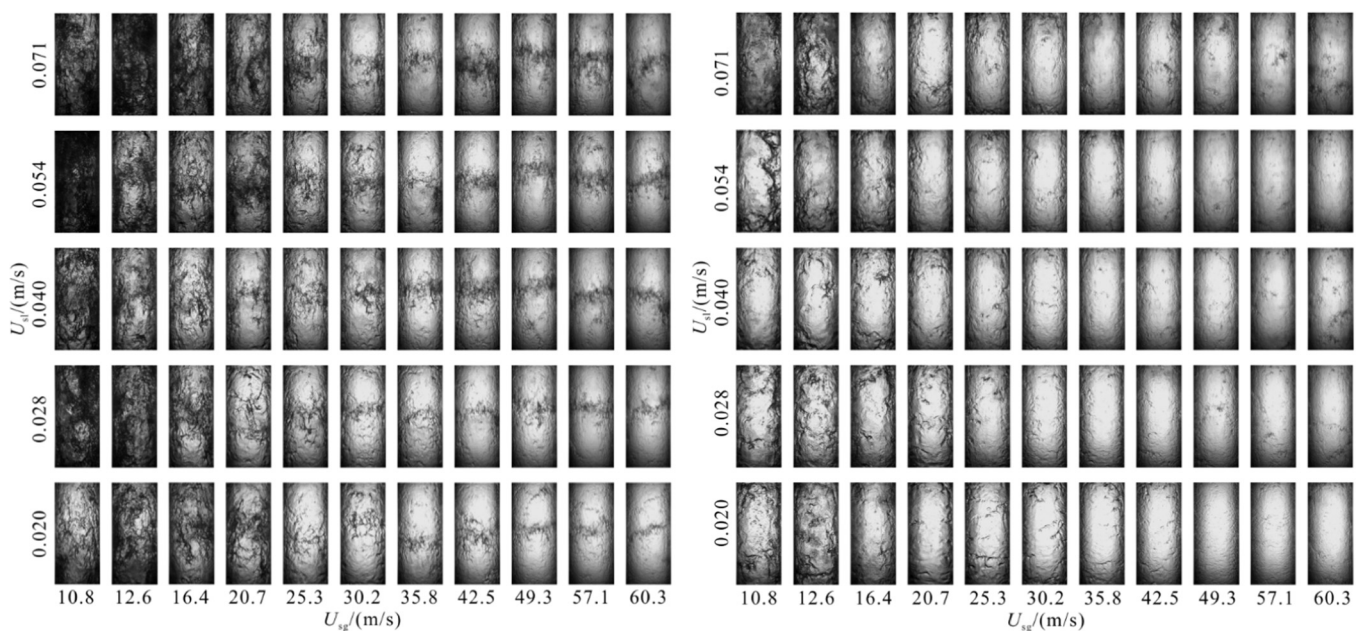


**Fig. 4.** Distribution of wave and base liquid film with gas and liquid velocities (wave, picture on the left side; base liquid film, picture on the right side).

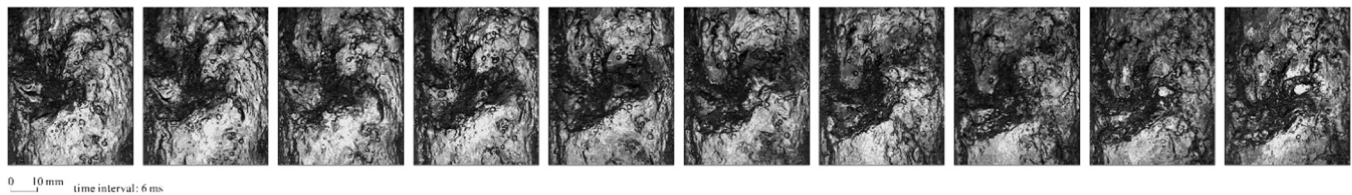


**Fig. 5.** Large wave roll and overturn leading to bubble entrainment (churn flow,  $U_{sg} = 10.8 \text{ m/s}$ ,  $U_{sl} = 0.054 \text{ m/s}$ ).

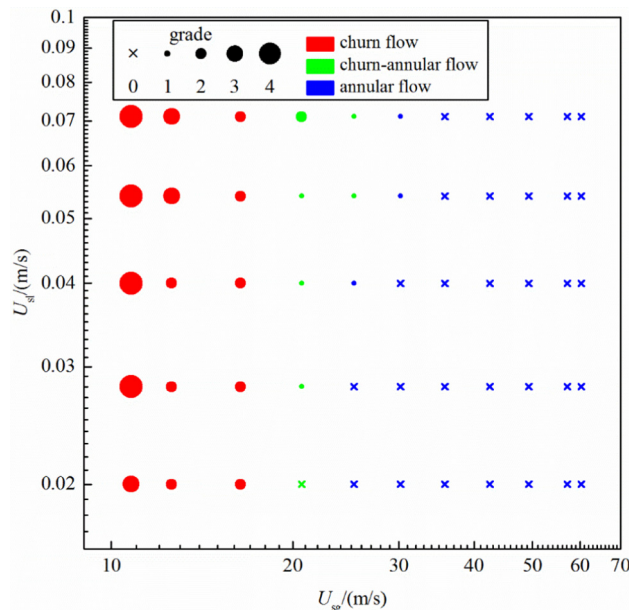


**Fig. 6.** Intensity distribution of bubble entrainment due to the large wave roll and overturn versus gas and liquid velocities.

roll and overturn, the synchronized bubble entrainment along with droplet entrainment, and droplets from the gas core impacting the liquid film.

### 3.1.1. Definition

#### (1) Large wave roll and overturn

In churn flow, huge waves on the liquid film roll and overturn rather than move unidirectionally upwards (Fig. 5). Part of the gas in the gas core is trapped in the huge wave and breaks up into small bubbles which are then distributed into the neighboring region of the liquid film (Video 1 in the Appendix). The following ability of bubbles with different sizes is different. Small bubbles are more likely to remain in the base liquid film. Large bubbles will burst rapidly even when they remain.

The large size of the huge wave leads to a large volume of entrapped gas during the single entrainment process. At the same time, the continuous liquid phase distribution range of the huge wave is large, which provides a suitable place for the dispersion of entrained gas after breaking. Therefore, this entrainment process often occurs under large liquid velocities where the flow regime is

churn flow (Fig. 6). It does not occur in annular flow. In churn flow, the superficial liquid velocity has little effect on the intensity of this entrainment process. With the increase in the superficial gas velocity, its intensity decreases (Fig. 6).

#### (2) Synchronized bubble entrainment along with droplet entrainment

The synchronized bubble entrainment along with droplet entrainment occurs only in two kinds of droplet entrainment: the bag break-up of waves and the ligament break-up of waves. A detailed discussion of these two kinds of droplet entrainment will be given in Section 3.2.

For bag break-up, after the opening bag of the lower part of the wave bursts, part of the gas remains in the bag and is dispersed into bubbles (Fig. 7, Video 2 in the Appendix). Bubbles are often distributed in the liquid film near the root of the bag. At the same time, the relatively large droplet that is generated by the bag break-up impacts the nearby liquid film, which also leads to a small amount of entrained bubbles.

For ligament break-up, the generated droplets impact the nearby liquid film leading to a small amount of entrained bubbles (Fig. 8, Video 3 in the Appendix). This synchronized bubble entrainment can only occur under proper conditions. Only when droplets of suitable size are deposited downstream of the wave at a speed greater than the wave velocity and then impinge on a liquid film of the appropriate thickness can a small number of bubbles be entrapped. At this time, the droplet deposition process is similar to the ducks and drakes. Droplets impact and jump on the liquid film many times, and the impact strength decreases gradually. Bubble entrainment occurs at the impact point. In contrast, larger droplets will deposit and reintegrate into the liquid film; smaller droplets will migrate into the gas core at a higher speed without in situ deposition. The thin liquid film cannot provide a suitable site for entrained bubbles.

Droplet entrainment is the premise of synchronized bubble entrainment. In addition, it has stringent requirements for the thickness of the liquid film at the entrainment position of droplets, as mentioned above. These make the intensity weak and the occurrence range limited. It occurs in the annular flow if the superficial gas velocity is not too large and the superficial liquid velocity is sufficiently large (Fig. 9).

#### (3) Droplets from gas core impacting the liquid film

Different from synchronized bubble entrainment along with droplet entrainment, the droplets inducing bubble entrainment are created from the gas core instead of the nearby broken waves.

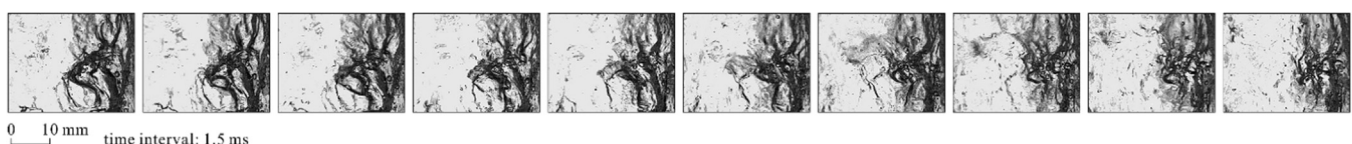


**Fig. 7.** Synchronized bubble entrainment along with bag break-up (churn flow,  $U_{sg} = 10.8 \text{ m/s}$ ,  $U_{sl} = 0.028 \text{ m/s}$ ).

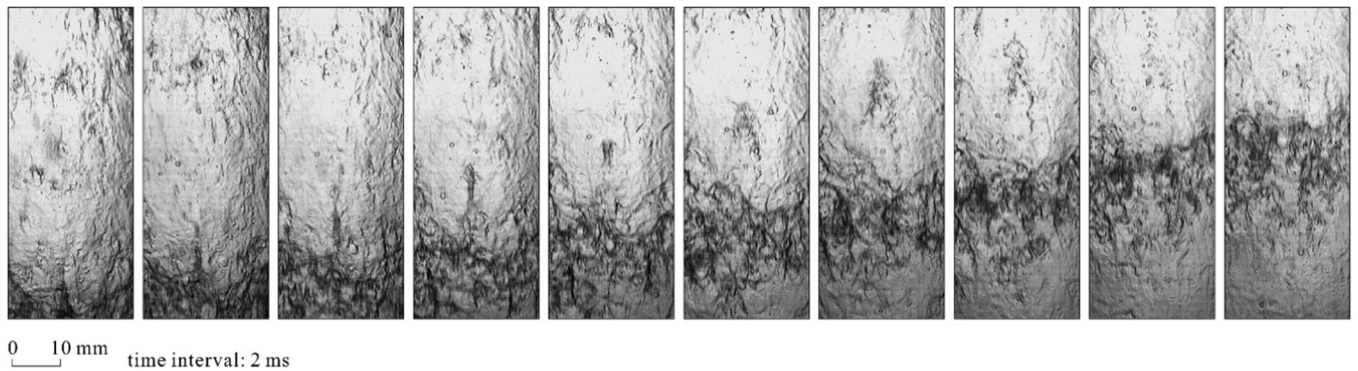


**Fig. 8.** Synchronized bubble entrainment along with ligament break-up (annular flow,  $U_{sg} = 35.8 \text{ m/s}$ ,  $U_{sl} = 0.071 \text{ m/s}$ ).

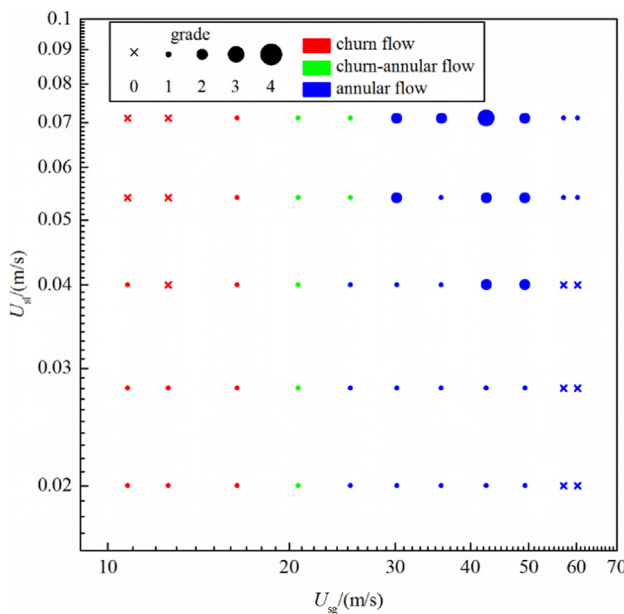


**Fig. 9.** Intensity distribution of bubble entrainment due to droplet entrainment versus gas and liquid velocities.

The droplet velocity is clearly larger, and the impact on the liquid film is enhanced. As a result, the initial impact of droplets in this process is stronger, which results in an increase in the axial range of the impact zone and a decrease in the circumferential range. Similarly, only droplets of a suitable size can play ducks and drakes (Fig. 10, Video 4 in the Appendix). Bubble entrainment often only occurs under the initial impact.

To meet the requirements of droplets and liquid film, this entrainment often occurs when the superficial gas velocity is moderate and the superficial liquid velocity is large enough. For

instance, it occurs in churn-annular flow when the superficial liquid velocity is large and in annular flow (Fig. 11).

### 3.1.2. Contrast between different bubble entrainments

Entrainment can be divided into primary entrainment and secondary entrainment. Primary entrainment is directly caused by the interaction between continuous gas and liquid phases. Secondary entrainment is a synchronous accompanying process of the primary entrainment. For the above three kinds of bubble entrainment, the large wave roll and overturn belong to primary entrainment, while the other two processes belong to secondary entrainment.

The number of entrained bubbles of the large wave roll and overturn is significantly larger than that of the other two processes. This is due to the difference in the trapping ability and the capacity of the liquid phase for bubbles. The size of the entrained bubbles of the large wave roll is also larger than that of the other two processes. For the secondary bubble entrainment, the bubble diameter is equivalent to the thickness of the base liquid film thickness. As to the stability of the entrained bubbles, the remaining bubbles in the base liquid film for the primary entrainment are easy to burst, and the bubbles resulting from the secondary entrainment are relatively stable.

### 3.1.3. Comparison with bubble entrainment in the horizontal flow

Overtaking of the fast ripples does not happen in the vertical flow, which is the primary bubble entrainment in horizontal flow (Hann et al., 2018). This is due to the difference between the effect of gravity on waves in horizontal and vertical flows. For example, the key phenomena in vertical flow such as flooding and flow reversal do not exist in horizontal flow. In horizontal flow, the wave folds to the wall under gravity. The folding direction of the wave is opposite to the direction of wave generation, which is beneficial to trapping gas. In vertical flow, gravity causes wave crests to fold downward where complete traps cannot form.

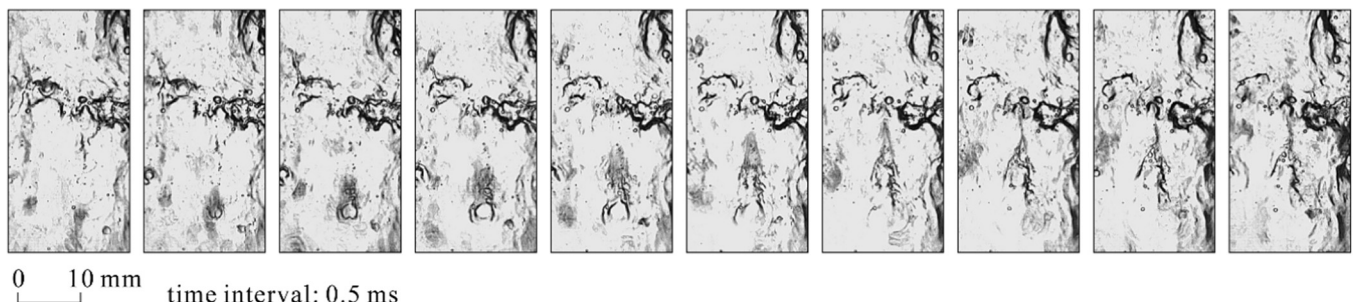


**Fig. 10.** Droplets from gas core impacting liquid film (churn flow,  $U_{sg} = 10.8 \text{ m/s}$ ,  $U_{sl} = 0.028 \text{ m/s}$ ).

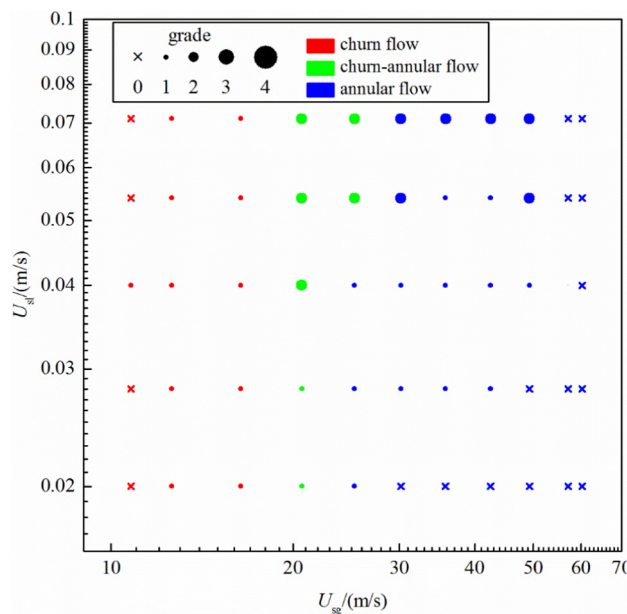


**Fig. 11.** Intensity distribution of bubble entrainment due to droplets from gas core impacting liquid film versus gas and liquid velocities.

### 3.2. Droplet entrainment

Five kinds of droplet entrainment were observed in the churn and annular flows within the experimental range: the shearing-off of waves containing bubbles, the bag break-up of waves, the ligament break-up of waves, droplets impacting the liquid film, and the burst of bubbles.

#### 3.2.1. Definition

##### (1) Shearing-off of waves containing bubbles

The cross-sectional area of the gas core decreases due to the existence of large waves, which results in larger gas velocity. The shearing ability of the gas increases with the increase in the gas velocity. In addition, entrained bubbles reduce the strength of the wave itself. The strength is regarded as a measure of resistance of the wave in breaking-up. These two aspects lead to the shearing-off of waves containing bubbles and the breakdown into clusters of droplets (Fig. 12, Video 5 in the Appendix).

One of the preconditions for the occurrence of this bubble entrainment is that the wave contains a large number of bubbles. This often corresponds to the flow conditions of the large wave roll and overturn. Therefore, the higher the superficial liquid velocity the greater the intensity of this droplet entrainment in churn and churn-annular flows (Fig. 13). However, this droplet entrainment does not exist in annular flow.

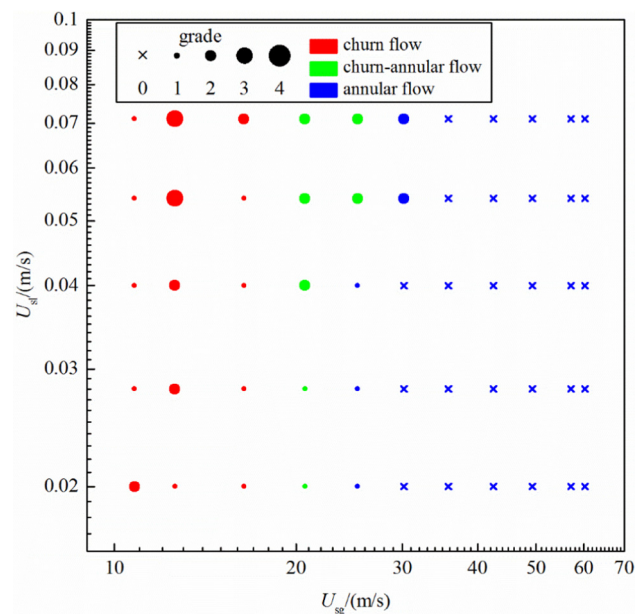


**Fig. 13.** Intensity distribution of droplet entrainment due to shearing-off of waves containing bubbles versus gas and liquid velocities.

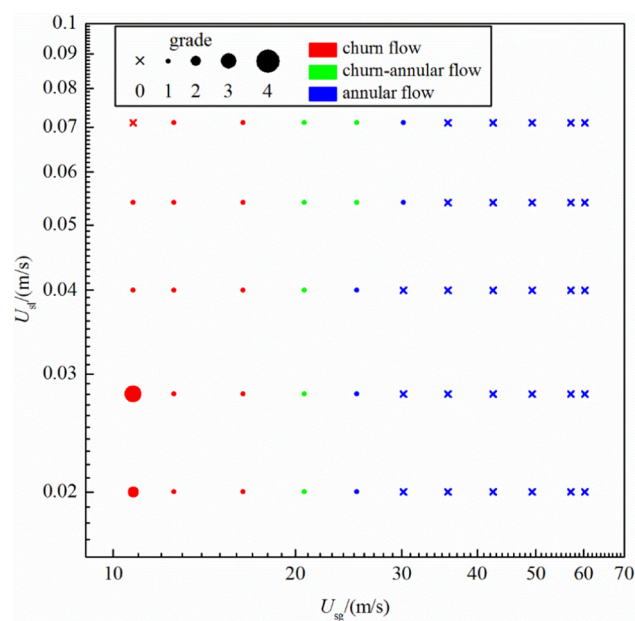


**Fig. 14.** Intensity distribution of droplet entrainment due to bag break-up of waves versus gas and liquid velocities.

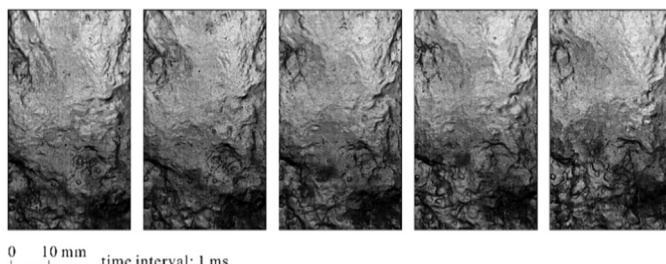


**Fig. 12.** Shearing-off of waves containing bubbles (churn flow,  $U_{sg} = 12.6 \text{ m/s}$ ,  $U_{sl} = 0.071 \text{ m/s}$ ).

## (2) Bag break-up of waves

The bag can be formed only when the wave size is appropriate. The gas accumulates continuously in the bag. When the pressure inside the bag increases to a certain extent, the bag will burst (Fig. 7, Video 2 in the Appendix). The thickness of the main part of the bag is small leading to the formation of droplet clusters with small size droplets when the bag is broken. The lower bag openings are thick and often break into short strips, which are deposited on the liquid film instead of flying into the gas core.

Generally, the intensity of this droplet entrainment is not strong. It can only occur in annular flows with low superficial gas velocities when the transverse size of the wave meets certain requirements. At a fixed superficial gas velocity, the intensity of this process varies little with the superficial liquid velocity (Fig. 14).

## (3) Ligament break-up of waves

In the region of wave aggregates, adjacent wave elements collide to form ligaments, which distribute along the axis. The ligament ruptures under the action of the gas core, which results in entrained droplets (Fig. 8, Video 3 in the Appendix and Fig. 15, Video 6 in the Appendix).

At relatively small gas velocities, the wave element has a large transverse dimension and wave height. However, its velocity is low resulting in poor stability. In addition, it is easy for the wave elements to connect with each other to form thick and long ligaments (Fig. 15). The ligaments easily make contact with each other to form a continuous liquid-phase grid structure, which limits the chance of rupture. The size of the droplets that are generated in this condition is large, and the droplets usually migrate at a speed slightly larger than the velocity of the wave for a short period and then deposit rapidly and re-integrate into the liquid film.

At relatively large gas velocities, the wave element has a small size and wave height. The transverse dimension is significantly smaller than the axial dimension, and its velocity is high. The small volume of the contact liquid phase between wave elements leads to the formation of finer ligaments (Fig. 8). In the wave region, the frequency of ligament formation and breakdown increases significantly. The size of the droplets decreases, but the number of droplets increases significantly.

Azzopardi (1997) analogizes the break-up of a single droplet to find the ligament break-up mechanism of a single wave element. The wave element is assumed to form a transverse ligament that is perpendicular to the flow direction. However, the ligaments formed by the cross-collision of wave elements are longitudinal and parallel to the flow direction, as observed in the experiment. This may indicate that a single wave element is hard to break up alone without having collided with adjacent waves.

The ligament break-up of waves occurs mainly in annular flow (Fig. 16). With the increase in the superficial gas velocity, the aspect ratio of the wave elements decreases. The collisions between wave elements increase, and the ligaments form more

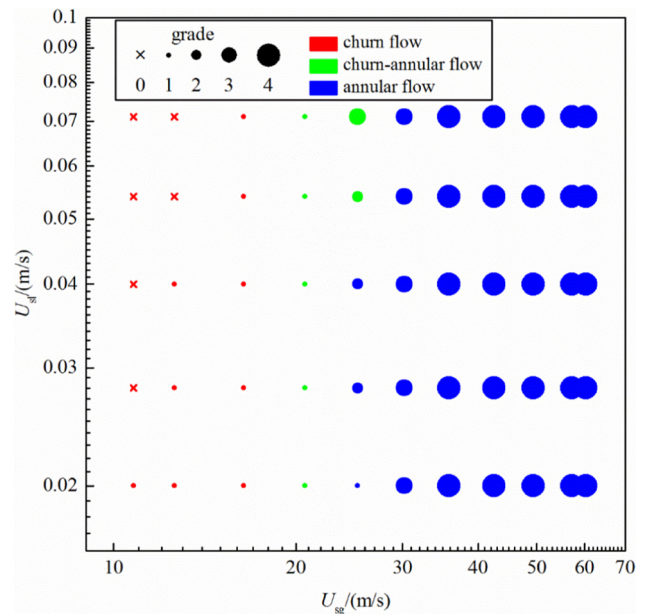


**Fig. 16.** Intensity distribution of droplet entrainment due to ligament break-up of waves versus gas and liquid velocities.

easily. At the same time, the high gas flow rate is more conducive to ligament breakage. Therefore, with the increase in the superficial gas velocity, the intensity of this entrainment increases gradually. At high gas velocities, the liquid velocity has little effect on the intensity of this entrainment (Fig. 16).

Comparing the intensity distribution of the bag break-up and the ligament break-up with gas and liquid velocities, it is found that the criteria for these two entrainment processes are basically the same as the transition criteria for churn flow and annular flow (Figs. 14 and 16). Moreover, there is not a strict criterion for the existence of a clear distinction between them. However, there is a coexistence area. This is due to the various waves that exist on the liquid film at a fixed gas-liquid flow rate (Fig. 4), and different waves result in different processes of droplet entrainment.

## (4) Droplets impacting the liquid film

The characteristics of droplet entrainment vary with the impact region of droplets. It is more likely to happen for droplets impacting in the wave region than those impacting in the base liquid film region. This is especially true for waves containing entrained bubbles.

Droplets impacting the base liquid film often experience a process of ducks and drakes (Fig. 17, Video 7 in the Appendix). Therefore, only a small number of small droplets can be generated in the gully region. When the droplets impact the wave, a crater is formed because the droplet directly impacts the front of the wave

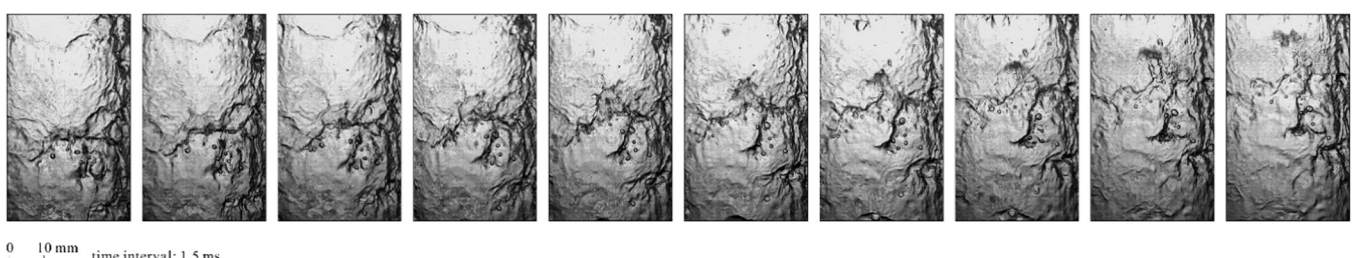


**Fig. 15.** Ligament break-up of waves leading to droplet entrainment ( $U_{sg} = 25.3 \text{ m/s}$ ,  $U_{sl} = 0.040 \text{ m/s}$ ).

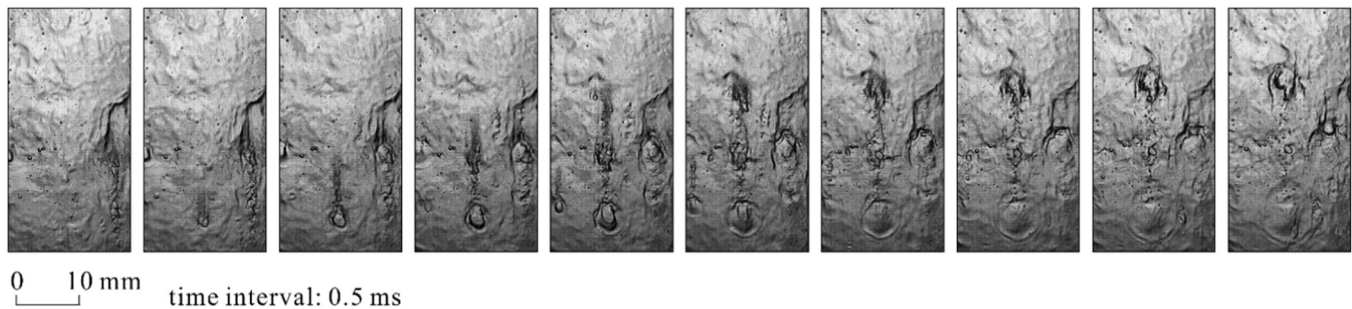


**Fig. 17.** Droplets impacting the base liquid film (churn-annular flow,  $U_{sg} = 20.7 \text{ m/s}$ ,  $U_{sl} = 0.054 \text{ m/s}$ ).

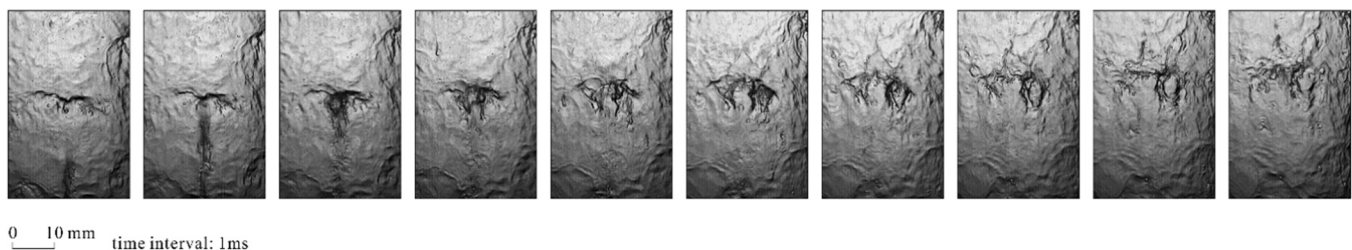


**Fig. 18.** Droplet impacting the wave (annular flow,  $U_{sg} = 25.3 \text{ m/s}$ ,  $U_{sl} = 0.040 \text{ m/s}$ ).

where the wave height is larger than the droplet diameter (Fig. 18, Video 8 in the Appendix). The impacting part of the waves deforms and ruptures. The wave parts on both sides of the impact site are likely to form small ligaments and then break up into droplets.

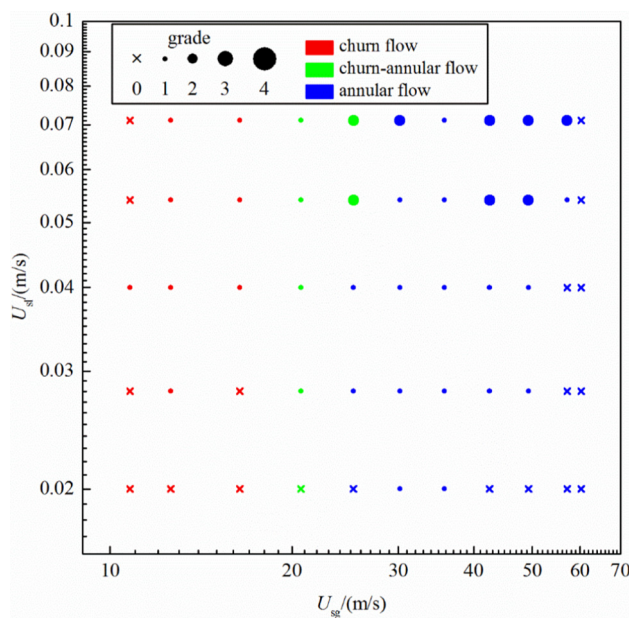


**Fig. 19.** Intensity distribution of droplet entrainment due to droplets impacting the liquid film versus gas and liquid velocities.

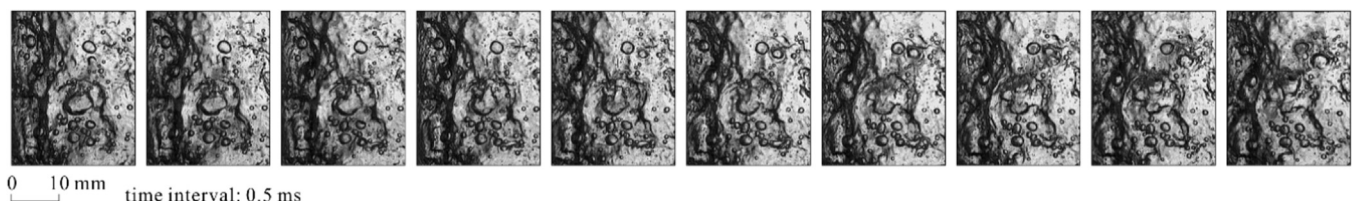


**Fig. 20.** Burst of bubbles leading to droplet entrainment (churn flow,  $U_{sg} = 12.6 \text{ m/s}$ ,  $U_{sl} = 0.020 \text{ m/s}$ ).

Although this entrainment occurs in the whole experimental range, its contribution to the number of droplets in the gas core is limited. Only when the superficial gas velocity is moderate and the superficial liquid velocity is large enough can the intensity of this entrainment be enhanced to a certain extent (Fig. 19).

### (5) Burst of bubbles

Some entrained bubbles remain in the base liquid film without following the moving wave. Because of the thin liquid film thickness, the bubble is easy to break up leading to droplet entrainment (Fig. 20, Video 9 in the Appendix).

This entrainment can only occur when the bubble size is approximately equal to the liquid film thickness. Therefore, it only occurs in churn and churn-annular flows at low intensity (Fig. 21).

#### 3.2.2. Contrast between different droplet entrainments

Droplet entrainment can also be divided into primary entrainment and secondary entrainment. The shearing-off of waves containing bubbles, bag break-up of waves and ligament break-up of waves belong to the primary entrainment, while the other two processes belong to the secondary entrainment.

For the number of entrained droplets, the contribution of shearing-off of waves containing bubbles and the ligament break-up of waves is the greatest, while the contribution of the bag break-up of waves is less. The other two secondary entrainment processes contribute the least. Therefore, the primary entrainment is the dominant entrainment in churn and annular flows. The droplet entrainment in churn flow is dominated by the shearing-off of waves containing bubbles, and the droplet

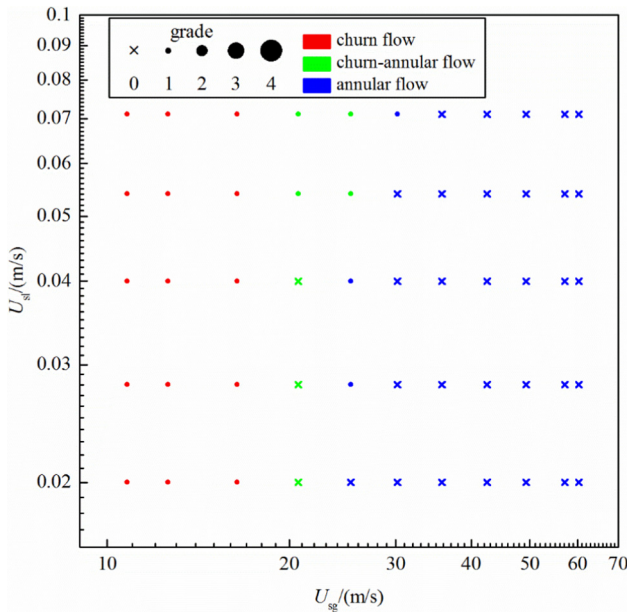


**Fig. 21.** Intensity distribution of droplet entrainment due to burst of bubbles versus gas and liquid velocities.

entrainment in annular flow is dominated by the ligament break-up of waves.

For the size of entrained droplets, the smaller the superficial gas velocity the larger the size of entrained droplets. The size of droplets is also affected by the structural characteristics of the broken liquid phase unit. At low gas velocities, the ligament is thicker, and the resulting droplets have a larger size. Most of the droplets that are generated by the bag break-up of waves come from the thin liquid wall of the bag, and their size is small. The shearing-off of waves containing bubbles results in small droplets, which often form a cluster.

For the initial velocity of the entrained droplets, in general, the higher the superficial gas velocity the higher the initial velocity of

entrained droplets. The initial velocity of droplets generated by primary entrainment is significantly higher than that of droplets generated by secondary entrainment.

### 3.2.3. Comparison with droplet entrainment in the horizontal flow

Bag break-up and ligament break-up coexist in a horizontal flow (Cherdantsev et al., 2014). In the vertical flow, although the bag break-up and ligament break-up coexist in a certain range of flow, the ligament break-up is usually dominant, and the bag break-up is auxiliary. In addition, the criteria for these two entrainments differ substantially for horizontal and vertical flows. This is probably due to the influence of gravity on the wave shape, which leads to the difference in the formation conditions of the bag and the ligament in horizontal and vertical flows.

### 3.3. Relationship between bubble entrainment and droplet entrainment

The intensity distribution of every possible entrainment is shown in Fig. 22 when the flow pattern changes from churn flow to annular flow at a fixed superficial liquid velocity of 0.054 m/s. The symbol for each entrainment process is listed below.

B1 symbolizes large wave roll and overturn, B2 symbolizes synchronized bubble entrainment along with droplet entrainment, and B3 symbolizes droplets from the gas core impacting the liquid film. D1 symbolizes shearing-off of waves containing bubbles, D2 symbolizes bag break-up of waves, D3 symbolizes ligament break-up of waves, D4 symbolizes droplets impacting the liquid film, and D5 symbolizes the burst of bubbles.

The dominant entrainment for both bubble and droplet changes when the flow pattern transits from churn flow to annular flow (Fig. 22). For bubble entrainment, the dominant entrainment changes from large wave roll and overturn (B1) to synchronized bubble entrainment along with droplet entrainment (B2) and droplets from the gas core impacting the liquid film (B3). This is a change from primary entrainment to secondary entrainment, which indicates a decreasing intensity of bubble entrainment. For droplet entrainment, the dominant entrainment changes from

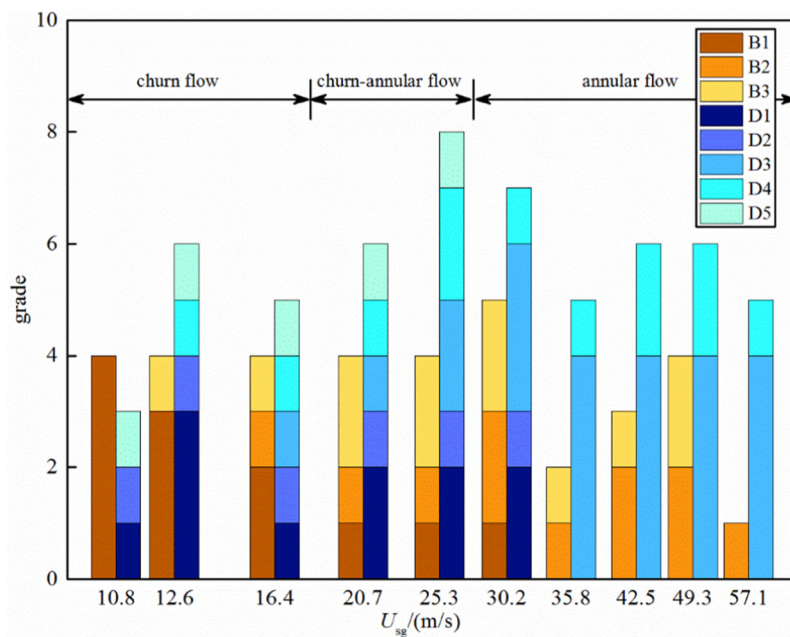


**Fig. 22.** Entrainment intensity variation versus gas velocity at the liquid velocity of 0.054 m/s.

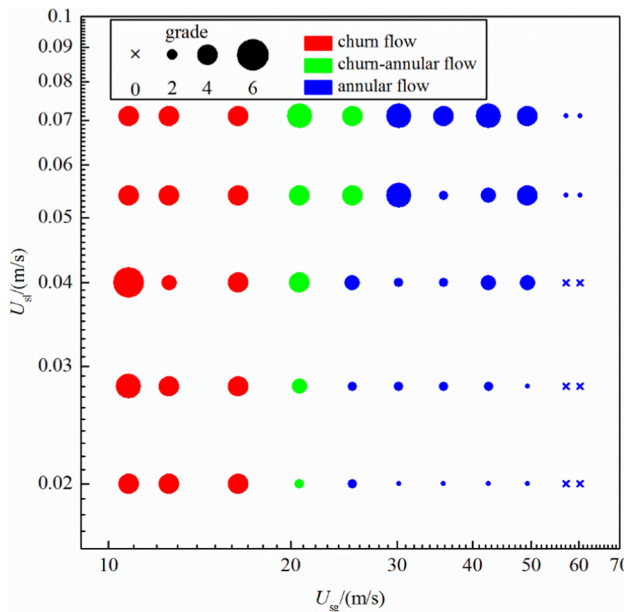


**Fig. 23.** Bubble entrainment regime map for churn and annular flows.

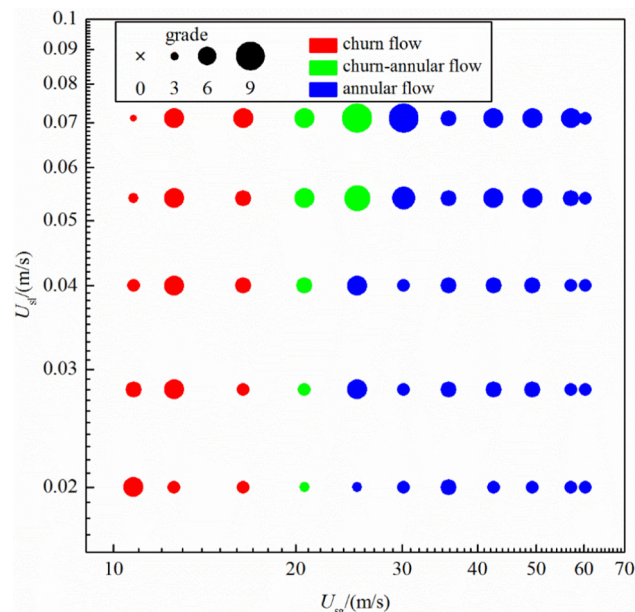


**Fig. 24.** Droplet entrainment regime map for churn and annular flows.

shearing-off of waves containing bubbles (D1) to ligament break-up of waves (D3).

Primary bubble entrainment is often the inducement of secondary droplet entrainment. Similarly, primary droplet entrainment is often the cause of secondary bubble entrainment. Fig. 22 indicates the specific relevance between these entrainments.

The large wave roll and overturn (B1) is beneficial to shearing-off of waves containing bubbles (D1) because the entrained bubbles reduce the strength of the wave. Both large wave roll and overturn (B1) and synchronized bubble entrainment along with droplet entrainment (B2) are helpful to the burst of bubbles (D5). The larger the number of large-sized bubbles generated by bubble entrainment, the greater the possibility of bubble breakup. The synchronized bubble entrainment along with droplet entrainment (B2) benefits from the bag break-up of waves (D2) and the ligament break-up of waves (D3) within a limited flow range. At high gas velocities, the intensity of B2 decreases because the generated droplets prefer flying into the gas core to redepositing back into the liquid film. The bag break-up of waves (D2) can be approximated as an incomplete version of the large wave roll and overturn (B1) where the low superficial liquid velocity keeps the bag open and thins the liquid film of the bag.

#### 4. Bubble and droplet entrainment regime map

The entrainment regime maps for bubble and droplet are constructed based on the global intensity distribution of every defined entrainment in Section 3.

At low superficial liquid velocities ( $U_{sl} = 0.02\text{--}0.028 \text{ m/s}$ ), the intensity of bubble entrainment decreases with the increase in the superficial gas velocity. There is no bubble entrainment in annular flow when the superficial gas velocity is high enough (Fig. 23). At high superficial liquid velocities ( $U_{sl} = 0.04\text{--}0.071 \text{ m/s}$ ), the intensity of bubble entrainment increases slightly, or remains unchanged with the increase in the superficial gas velocity, and it then decreases gradually. The smaller the superficial gas velocity, the greater the degree of weakening of bubble entrainment intensity with the increase in the superficial gas velocity.

In churn flow, the superficial liquid velocity has little effect on the intensity of bubble entrainment at fixed liquid velocities. In churn-annular and annular flows, the intensity of bubble entrainment increases with increasing superficial liquid velocity at fixed superficial gas velocities (Fig. 23).

These changes are caused by the two necessary conditions for bubble entrainment. On the one hand, bubble entrainment requires a large enough range of continuous liquid phase to provide distribution occasions for bubbles. On the other hand, bubble entrainment requires strong gas-liquid interactions to ensure sufficient gas entrainment. The greater the superficial gas velocity, the more advantageous it is to the second aspect, and the more disadvantageous it is to the first aspect. The effect of the superficial liquid velocity is opposite. Therefore, the intensity distribution of the bubble entrainment is determined by the degree of change in the above two aspects when the gas and liquid velocities are varied.

At fixed superficial liquid velocities, the intensity of the droplet entrainment first decreases, then increases, then decreases again slightly (Fig. 24). At fixed superficial liquid velocities, the intensity of the droplet entrainment is lower than that in adjacent churn flow and annular flow.

At low superficial gas velocities ( $U_{sg} = 10.8 \text{ m/s}$ ), the intensity of the droplet entrainment decreases with the increase in the superficial liquid velocity. At high superficial gas velocities ( $U_{sg} = 12.6\text{--}60.3 \text{ m/s}$ ), the intensity of the droplet entrainment increases with the increasing superficial liquid velocity at fixed superficial gas velocities. Moreover, the degree of increase increases first and then decreases with the increasing superficial gas velocity.

In comparing bubble entrainment and droplet entrainment, it is found that there is no bubble entrainment in the annular flow if the superficial gas velocity is high and the superficial liquid velocity is low. Droplet entrainment occurs in the whole flow conditions.

#### 5. Conclusions

- (1) There are three kinds of bubble entrainment processes and five kinds of droplet entrainment processes in vertical churn and annular flows. They can be divided into two categories: primary entrainment and secondary entrainment. The pri-

- mary entrainment includes one kind of bubble entrainment, which is large wave roll and overturn, and three kinds of droplet entrainment, which are shearing-off of waves containing bubbles, bag break-up of waves and ligament break-up of waves. The secondary entrainment includes two kinds of bubble entrainment, which are synchronized bubble entrainment along with droplet entrainment and droplets from the gas core impacting the liquid film, and two kinds of droplet entrainment, which are droplets impacting the liquid film and burst of bubbles.
- (2) During the flow regime transition from churn flow to annular flow, the dominant bubble entrainment changes from the large wave roll and overturn to the synchronized bubble entrainment along with droplet entrainment; the dominant droplet entrainment changes from shearing-off of waves containing bubbles to ligament break-up of waves.
  - (3) There is a close relationship between bubble entrainment and droplet entrainment. The bubbles generated by the bubble entrainment reduce the strength of large-scale waves and facilitate the shearing-off of waves. A small amount of droplets are entrained due to the burst of the residual bubbles in the liquid film. Under appropriate conditions, droplets generated by the bag and ligament break-up of waves can directly impact the liquid phase leading to synchronous bubble entrainment. A small amount of bubbles can be entrapped by droplets from the gas core impacting the liquid film.
  - (4) The primary entrainment intensity is significantly greater than that of the secondary entrainment. During the transition from churn to annular flow, the change in primary entrainment intensity determines the intensity of the secondary entrainment.

## Declaration of Competing Interest

None.

## Acknowledgments

This work was supported by the National Natural Science Foundation–Outstanding Youth Foundation (51622405), the 973 Program (2015CB251200), the National Science and Technology Major Project (2016ZX05028-001-03), the Natural Science Foundation of Shandong Province (JQ201716) and the National Engineering Laboratory for Testing and Detection Technology of Subsea Equipments.

## Appendix A. Supplementary data

There are nine videos. The window width corresponds to the tube diameter, which is 0.05 m. The frame rate is 5 fps, which is 1/400 of the actual rate. Supplementary data to this article can be found online at <https://doi.org/10.1016/j.ces.2019.05.005>.

## References

- Alekseenko, S.V., Cherdantsev, A.V., Heinz, O.M., Kharlamov, S.M., Markovich, D.M., 2014. Analysis of spatial and temporal evolution of disturbance waves and ripples in annular gas–liquid flow. *Int. J. Multiph. Flow* 67, 122–134.
- Alipchenkov, V.M., Nigmatulin, R.I., Soloviev, S.L., Stonik, O.G., Zaichik, L.I., Zeigarnik, Y.A., 2004. A three-fluid model of two-phase dispersed-annular flow. *Int. J. Heat Mass Transf.* 47 (24), 5323–5338.
- Azzopardi, B.J., 1983. Mechanisms of Entrainment in Annular Two Phase Flow. UKAEA Atomic Energy Research Establishment, Oxfordshire.
- Azzopardi, B.J., 1997. Drops in annular two-phase flow. *Int. J. Multiph. Flow* 23, 1–53.
- Azzopardi, B.J., Wren, E., 2004. What is entrainment in vertical two-phase churn flow? *Int. J. Multiph. Flow* 30 (1), 89–103.
- Berna, C., Escrivá, A., Muñoz-Cobo, J.L., Herranz, L.E., 2014. Review of droplet entrainment in annular flow: Interfacial waves and onset of entrainment. *Prog. Nucl. Energy* 74 (3), 14–43.
- Cherdantsev, A.V., 2018. Overview of physical models of liquid entrainment in annular gas–liquid flow. *AIP Conf. Proc.* 1939 (1), 020006.
- Cherdantsev, A.V., Hann, D.B., Azzopardi, B.J., 2014. Study of gas-sheared liquid film in horizontal rectangular duct using high-speed LIF technique: three-dimensional wavy structure and its relation to liquid entrainment. *Int. J. Multiph. Flow* 67, 52–64.
- Cioncolini, A., Thome, J.R., 2010. Prediction of the entrained liquid fraction in vertical annular gas–liquid two-phase flow. *Int. J. Multiph. Flow* 36 (4), 293–302.
- Crowe, C.T., 2005. *Multiphase Flow Handbook*. Crc Press, Boca Raton.
- Dasgupta, A., Chandraker, D.K., Kshirasagar, S., Reddy, B.R., Rajalakshmi, R., Nayak, A.K., Walker, S.P., Vijayan, P.K., Hewitt, G.F., 2017. Experimental investigation on dominant waves in upward air–water two-phase flow in churn and annular regime. *Exp. Therm Fluid Sci.* 81, 147–163.
- Durve, A.P., Patwardhan, A.W., 2012. Numerical and experimental investigation of onset of gas entrainment phenomenon. *Chem. Eng. Sci.* 73, 140–150.
- Hann, D.B., Cherdantsev, A.V., Azzopardi, B.J., 2018. Study of bubbles entrapped into a gas-sheared liquid film. *Int. J. Multiph. Flow* 108, 181–201.
- Hewitt, G.F., 2012. Churn and wispy annular flow regimes in vertical gas–liquid flows. *Energy Fuels* 26 (7), 4067–4077.
- Hewitt, G.F., Hall Taylor, N.S., 1970. *Annular Two-Phase Flow*. Elsevier, UK.
- Isaenkov, S.V., Cherdantsev, A.V., Vozhakov, I.S., Cherdantsev, M.V., Arkhipov, D.G., Markovich, D.M., 2019. Study of primary instability of thick liquid films under strong gas shear. *Int. J. Multiph. Flow* 111, 62–81.
- Ishii, M., Grolmes, M.A., 1975. Inception criteria for droplet entrainment in two-phase concurrent film flow. *AIChE J.* 21, 308–318.
- Ishii, M., Mishima, K., 1989. Droplet entrainment correlation in annular two-phase flow. *Int. J. Heat Mass Transf.* 32 (10), 1835–1846.
- Kataoka, I., Ishii, M., Nakayama, A., 2000. Entrainment and deposition rates of droplets in annular two-phase flow. *Int. J. Heat Mass Transf.* 43 (9), 1573–1589.
- Kumar, P., Das, A.K., Mitra, S.K., 2016. Physical understanding of gas–liquid annular flow and its transition to dispersed droplets. *Phys. Fluids* 28 (7), 072101.
- Kunugi, T., 2017. Summary: study on wavy interface behavior and droplet entrainment of annular two-phase flow in rod bundle geometry with spacers. *Nucl. Eng. Des.*, 45–53
- Liu, L., Bai, B., 2017. Generalization of droplet entrainment rate correlation for annular flow considering disturbance wave properties. *Chem. Eng. Sci.* 164, 279–291.
- Mishima, K., Ishii, M., 1984. Flow regime transition criteria for upward two-phase flow in vertical tubes. *Int. J. Heat Mass Transf.* 27 (5), 723–737.
- Miwa, S., Moribe, T., Tsutsumi, K., Hibiki, T., 2018. Experimental investigation of air entrainment by vertical plunging liquid jet. *Chem. Eng. Sci.* 181, 251–263.
- Pan, L., Hanratty, T.J., 2002. Correlation of entrainment for annular flow in vertical pipes. *Int. J. Multiph. Flow* 28 (3), 363–384.
- Patruno, L.E., Dorao, C.A., Svendsen, H.F., Jakobsen, H.A., 2009. On the modelling of droplet–film interaction considering entrainment, deposition and breakage processes. *Chem. Eng. Sci.* 64 (6), 1362–1371.
- Patruno, L.E., Marchioro Ystad, P.A., Jenssen, C.B., Marchetti, J.M., Dorao, C.A., Svendsen, H.F., Jakobsen, H.A., 2010. Liquid entrainment–Droplet size distribution for a low surface tension mixture. *Chem. Eng. Sci.* 65 (18), 5272–5284.
- Pham, S.H., Kawara, Z., Yokomine, T., Kunugi, T., 2014. Detailed observations of wavy interface behaviors of annular two-phase flow on rod bundle geometry. *Int. J. Multiph. Flow* 59 (2), 135–144.
- Pham, S.H., Kawara, Z., Yokomine, T., Kunugi, T., 2015. Measurements of liquid film and droplets of annular two-phase flow on a rod-bundle geometry with spacer. *Int. J. Multiph. Flow* 70, 35–57.
- Rodriguez, D.J., Shedd, T.A., 2004. Entrainment of gas in the liquid film of horizontal, annular, two-phase flow. *Int. J. Multiph. Flow* 30 (6), 565–583.
- Salque, G., Gajan, P., Strzelecki, A., Couput, J.P., El-Hima, L., 2013. Atomisation rate and gas/liquid interactions in a pipe and a venturi: influence of the physical properties of the liquid film. *Int. J. Multiph. Flow* 51, 87–100.
- Sawant, P., Ishii, M., Mori, M., 2008. Droplet entrainment correlation in vertical upward co-current annular two-phase flow. *Nucl. Eng. Des.* 238 (6), 1342–1352.
- Schubring, D., Ashwood, A.C., Shedd, T.A., Hurlburt, E.T., 2010. Planar laser-induced fluorescence (PLIF) measurements of liquid film thickness in annular flow. Part I: Methods and data. *Int. J. Multiph. Flow* 36 (10), 815–824.
- Taitel, Y., Bornea, D., Dukler, A.E., 1980. Modelling flow pattern transitions for steady upward gas–liquid flow in vertical tubes. *AIChE J.* 26 (3), 345–354.
- Tekavčič, M., Končar, B., Kljenak, I., 2018. The concept of liquid inlet model and its effect on the flooding wave frequency in vertical air–water churn flow. *Chem. Eng. Sci.* 175, 231–242.
- Van 't Westende, J.M.C., 2008. Droplets in Annular-dispersed Gas-liquid Pipe-flows. Delft University of Technology, Netherlands.
- van Nimwegen, A.T., Portela, L.M., Henkes, R.A.W.M., 2015. The effect of surfactants on air–water annular and churn flow in vertical pipes. Part 1: Morphology of the air–water interface. *Int. J. Multiph. Flow* 71, 133–145.
- Wang, K., Bai, B., Ma, W., 2013a. Huge wave and drop entrainment mechanism in gas–liquid churn flow. *Chem. Eng. Sci.* 104, 638–646.
- Wang, K., Bai, B., Ma, W., 2013b. A model for droplet entrainment in churn flow. *Chem. Eng. Sci.* 104, 1045–1055.

- Wang, K., Ye, J., Bai, B., 2017. Entrained droplets in two-phase churn flow. *Chem. Eng. Sci.* 164, 270–278.
- Woodmansee, D.E., Hanratty, T.J., 1969. Mechanism for the removal of droplets from a liquid surface by a parallel air flow. *Chem. Eng. Sci.* 24, 299–307.
- Wu, B., Firouzi, M., Mitchell, T., Rufford, T.E., Leonardi, C., Towler, B., 2017. A critical review of flow maps for gas-liquid flows in vertical pipes and annuli. *Chem. Eng. J.* 326, 350–377.
- Xie, Z., Hewitt, G.F., Pavlidis, D., Salinas, P., Pain, C.C., Matar, O.K., 2017. Numerical study of three-dimensional droplet impact on a flowing liquid film in annular two-phase flow. *Chem. Eng. Sci.* 166, 303–312.
- Zhang, J., Chen, J.J., Zhou, N., 2012. Characteristics of jet droplet produced by bubble bursting on the free liquid surface. *Chem. Eng. Sci.* 68 (1), 151–156.